COMMUNICATION

Nanostructured Calcite Single Crystals with Gyroid Morphologies

By *Alexander S. Finnemore, Maik R. J. Scherer, Richard Langford, Sumeet Mahajan, Sabine Ludwigs, Fiona C. Meldrum,* and *Ullrich Steiner**

Nature's ability to fashion single crystals into nearly any shape is remarkable, and as yet unparalleled by current technology.[1] A beautiful example is provided by sea-urchin spines and skeletal elements, each of which has a complex, sponge-like structure, and yet is a single crystal of calcite.[2] In contrast, the unconstrained crystallization of calcium carbonate ($CaCO_3$) leads to the precipitation of brittle rhombohedral calcite crystals.

Biologically controlled mineralization depends on the interplay between a number of factors, including insoluble organic matrices, soluble biomacromolecules, and inorganic ions. The effects of these factors on $CaCO_3$ nucleation and growth, which can also lead to control over polymorph and orientation, have been investigated and demonstrated using a number of model systems. Precipitation in association with self-assembled[3,4] and Langmuir[5–7] monolayers has shown the potential of these insoluble matrices to direct crystal orientation and polymorph, while investigation of the effects of soluble additives, such as magnesium[8,9] and biomacromolecules,[10–12] have shown effects on crystal morphology and polymorph. It is becoming increasingly apparent that the formation of crystalline $CaCO_3$ is often preceded by an amorphous $CaCO_3$ precursor (ACC), which isotropically fills the growth-directing organic template before crystallizing.[13,14] Synthetic ACC nanoparticles form from free ions, coalesce, and then crystallize as calcite, aragonite, or vaterite via dehydration and mass transport.[15] The lifetime of the amorphous material is determined by the ionic concentration as well as surface functionalization and soluble organic macromolecules,[16,17] ranging from minutes to months according to the preparation conditions.

Mimicking the structures and properties of biominerals is a significant and challenging goal. Advances in synthetically replicating biological control over crystal morphologies include the preparation of single crystals with bicontinuous structures by templating sea-urchin skeletal plates[18–20] and the growth of calcite into monolayers of colloidal particles[21] and porous polymer films.[22,23] Significantly, it has been shown that ACC is extremely effective in penetrating and molding to templates, as shown by the formation of 50 μm porous single crystals of calcite with submicrometer features through the templating of three-dimensional colloidal crystals.[24] Macroscopic micropatterned calcite single crystals have also been grown via an ACC precursor by the controlled nucleation of ACC in a template patterned with regularly spaced pillars.[15] The release of stress, water, and impurities on the surfaces of a micrometer-sized structure during crystallization indicates the necessity of close-packed features when growing large single crystals from ACC.

The formation of finely structured biominerals relies on the presence of a suitable organic matrix, which effectively acts as a mold and thereby dictates the morphology of the product crystal. As an excellent analog of biological self-assembly, synthetic block copolymers are well known to spontaneously form a wide range of highly regular structures. Diblock copolymers, for example, self-assemble via phase separation of the chemically dissimilar blocks into periodic spherical, cylindrical, or lamellar arrays.[25] Particularly interesting is the triply periodic gyroid morphology.[26,27] The double gyroid forms when the minority polymer block has a volume fraction of 33–37%.[28] It consists of two continuous and intertwined, but non-intersecting worm-like networks, formed by the minority block (Fig. 1a), separated by a continuous matrix of the majority phase (Fig. 1c). The structure is a crystal-like ordered microphase with a unit cell on the nanometer scale, and is said to be tricontinuous. Degrading and dissolving the network material yields a porous, continuous template formed by the self-supporting matrix (Fig. 1c–f). This ordered sponge-like structure has a very high surface area in comparison to other copolymer morphologies and colloidal arrays, offering a rewarding platform for material processing. Interestingly, the triply periodic minimal surface (TPMS) of the double gyroid is strikingly similar to the sea-urchin skeletal structure, extracted and replicated by Lai et al. [29], albeit on a smaller length scale (Fig. 2c–d). That sea urchins produce skeletal plates with a TPMS structure is intriguing, and it has been speculated that this structure generates a porous mineral that is optimal for mechanical strength and fluid permeability.[29,30] Indeed, if bicontinuous two-phase composite materials are constructed from materials with differing transport properties, optimal transport performance through both materials is anticipated when a TPMS structure is adopted.[31]

Crystallization within a polymer replica of a sea urchin skeletal plate has been shown to yield single crystals with TPMS structures identical to those of the original urchin plate.[18–20] While highly effective in demonstrating that such complex

[*] Prof. U. Steiner, A. S. Finnemore, M. R. J. Scherer, R. Langford, Dr. S. Mahajan
Department of Physics, University of Cambridge
J. J. Thomson Avenue, CB3 0HE (UK)
E-mail: u.steiner@phy.cam.ac.uk
Dr. S. Ludwigs, Prof. U. Steiner
Freiburg Institute for Advanced Studies (FRIAS)
University of Freiburg D-79104 Freiburg (Germany)
Prof. F. C. Meldrum
School of Chemistry,
University of Leeds, Leeds LS2 9JT (UK)

DOI: 10.1002/adma.200900615

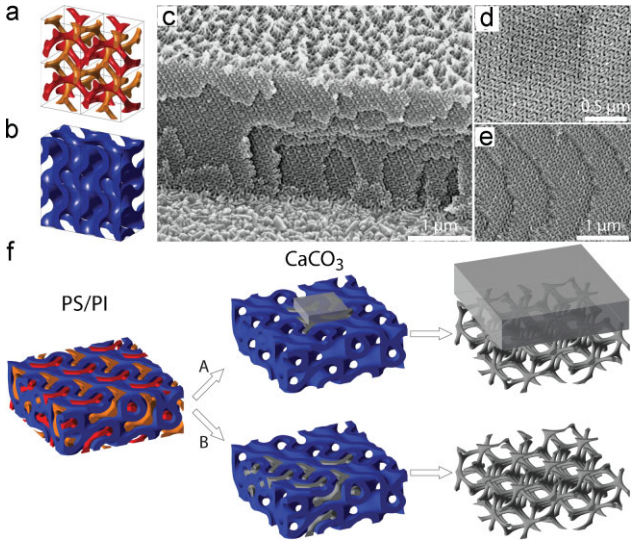

Figure 1. a) The two intertwined, non-intersecting gyroid networks (polyisoprene (PI), replicated by calcite). b) The sponge-like PS matrix. c) Cross-section of a patterned PS film showing the continuous matrix ((211) face) after PI removal, which exposes the two-gyroid networks for crystal infiltration. d–e) High-magnification images of the (421), and (100) cross-sectional fracture planes of the porous PS film, same magnification. f) Schematic representation of the crystallization process. Left to right: Films of the PS/PI copolymer self-assemble into a double-gyroid microphase morphology. After removal of the two PI networks (red and orange) from the PS matrix (blue), calcite crystals nucleate (A) on the surface of or (B) inside the polymer film and grow into the porous networks, leading to a gyroid-patterned single crystal, visible after PS matrix removal.

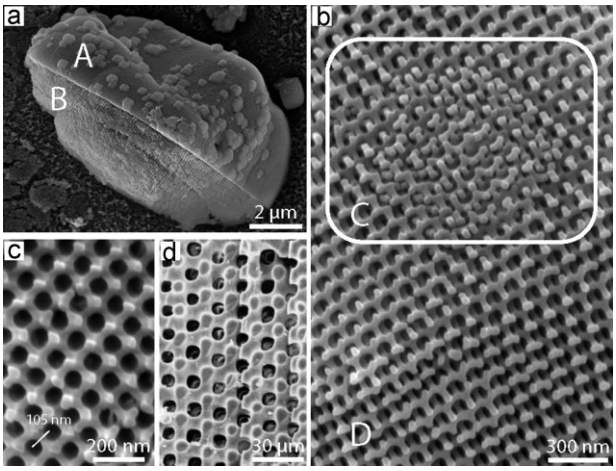

Figure 2. Calcite single crystal after PS removal. a) Side view of an (A) unstructured and (B) gyroid structured calcite single crystal arising from growth into a porous PS film as described in Figure 1f, Route A. The small facets on the unstructured section of the crystal arose from secondary crystal nucleation (see Experimental section), their coalignment serves as evidence for single crystallinity, while the poorly defined morphology of the parent crystal is consistent with precipitation via an amorphous crystallization precursor. b) Examples of the replication of the full double gyroid (both networks) and just a single network are shown and are marked C and D, respectively. c) A tilted zoom into b) shows the high quality with which the polymer template was replicated by the structured single crystal. Facet formation inside the gyroid-patterned crystal was not observed. d) An SEM image of the skeletal plate of a sea urchin that is also a single crystal of calcite and displays a similar morphology, albeit on a larger length scale, to the gyroid structure (from ref. [37]).

single-crystal morphologies can be accessed synthetically, this technique is limited by the requirement for the native biomineral as a starting material. Thus, the size of the product crystals is restricted to that of the original urchin plate, as is the geometry of the structure and pore sizes are invariably 10–15 μm in all echinoderms. In this work, we explore a very general route to producing single crystals with TPMS structures namely carrying out crystallization within a block-copolymer scaffold. This polymer template therefore provides access to these structures by a purely synthetic route, and also enables control over the structure and pore sizes. In the demonstration provided here, calcite single crystals with intricate TPMS structures were patterned on a 10 nm scale using a suitable structure-directing self-assembled polymer scaffold. To achieve a bicontinuous crystal morphology, the double-gyroid morphology of a polystyrene-*b*-polyisoprene (PS-*b*-PI) block copolymer was employed. Due to the narrowly defined chemical composition of the gyroid block-copolymer phase, a readily available lamellae-forming PS-*b*-PI was used, to which a low-molecular-weight polystyrene (PS) homopolymer was added. The incorporation (swelling) of the homopolymer into the PS phase of PS-*b*-PI is well known to modify the copolymer phase morphology.[32] By adding the required amount of PS to PS-*b*-PI solutions (see Experimental section), films exhibiting the gyroid morphology of continuous polyisoprene (PI) channels in a PS matrix were obtained. Subsequent exposure of the sample to UV light partially degrades the PI and cross-linked PS, thereby enabling the selective removal of PI by washing the sample in ethanol.[33,34] Figure 1c–e shows scanning electron microscopy (SEM) images of the PS-gyroid morphology after PI removal. The gyroid morphology not only exhibits a highly periodic surface reconstruction, but also spans the entire thickness (1–2 μm) of the film with the same regularity. The films were continuous over the whole 2 cm^2 substrate (see Experimental section).

Crystallization of $CaCO_3$ in association with the prepared copolymer films was carried out using the ammonium carbonate diffusion method, where the substrate was immersed in a solution of calcium chloride and exposed to ammonium carbonate vapor.[35] Methanol (20 vol%) was added to the solution to facilitate its infiltration into the gyroid structure, which otherwise exhibited a hydrophobic behavior. ACC has been shown to be highly effective in penetrating into small pores,[24] and its presence as a precursor species was investigated here by isolating precipitate produced in the bulk solution at early times. Analysis of precipitate isolated from solutions of concentrations 50 mM and above revealed sub-micrometer spherical particles, as is consistent with ACC. Raman spectra of this precipitate showed only broad peaks at 280 and 1100 cm^{-1}, respectively, confirming its amorphous nature (data not shown). At concentrations below 50 mM, the precipitate was found to be crystalline from even the earliest times. That ACC was only formed with any significant lifetime at higher solution concentrations, and was also supported by visual inspection of the reaction solutions, which were clear throughout the entire crystallization process for

concentrations <50 mM but were cloudy at concentrations above this. It is notable that the addition of ethanol to $CaCO_3$ growth solutions has been shown to stabilize ACC.[36] It is likely that the methanol added here exhibits a similar effect, increasing the lifetime of the precursor ACC phase as compared with purely aqueous solutions.

The influence of the $CaCl_2$ solution concentration on the product crystals was investigated over the range 10 mM–1 M. At low $CaCl_2$ concentrations (<50 mM), calcite rhombohedra nucleated on the surface of the PS film and began to grow into the gyroid pores. Interestingly, crystal growth into the template never exceeded 20 nm, regardless of the crystallization time. This behavior can be attributed to the absence of an ACC phase under these conditions. Without ACC, crystallization within the template must occur by diffusion of the reactant ions, which will inevitably be slow in the small pores. Further blocking of the small pores would be expected, limiting mass crystal growth. At higher $CaCl_2$ concentrations (50 mM–1 M), calcite growth deep into the self-assembled porous gyroid structure was observed, yielding calcite single crystals with an extended periodic nanostructure. The penetration depth increased with increasing ion concentration, that is, with increased ACC formation. One molar solutions produced calcite rhombohedra on the film surface after only 1 h. While previous experiments investigating growth of calcite into a template have achieved penetration into the template of less than 100 nm,[22,24] in the present study the crystals infiltrated several hundred nanometers through the organic template, as evidenced after PS removal (see Fig. 2a). Figure 2b presents a higher-magnification image of the calcite single crystal grown within the polymer template, and clearly shows the excellence of the templating process. Interestingly, templating was seen to replicate either only one (D) or both interpenetrating networks (C, see Fig. 1a for an explanation of the two networks). As the two networks of an ideal double-gyroid morphology do not intersect, there is no connection between them. This indicates that the accessibility of the network pores is of critical importance for their replication. Figure 2c shows a high-magnification image of a gyroid-patterned single crystal, clearly illustrating the well-defined replication of the polymer morphology. Figure 2d, showing the calcite extracted from a sea urchin, highlights the remarkable morphological similarity between the gyroid calcite and the urchin skeletal plate, albeit with rather different periodicities.

In addition to calcite that nucleated on top of the polymer film, calcite single crystals that nucleated and grew entirely within the self-assembled PS porous network were also observed. These crystals were completely porous and exhibited mesoscopic structures that were entirely dictated by the porous polymer matrix, as shown in Figure 3. While the majority of the crystal showed a periodic mesostructure in cross-section as a signature for the gyroid structure (Fig. 3a, c, and d), lifting of the crystal from the substrate and examination of the surface at the polymer film/substrate interface revealed a disordered structure (Fig. 3b, marked A). Close examination of this part of the structure revealed a local periodicity imposed by the copolymer but no long-range order. This arises from a surface reconstruction of the polymer self-assembly at this interface. The free surface of the crystal in Figure 3a does not show this disordered surface. This crystal has grown predominantly in a lateral (in-plane) fashion, with a growth preference along the diagonals characteristic of rhombohedral calcite. While the symmetry of the crystal lattice cannot be inferred from the local replicated morphology, the rhombohedral crystal symmetry is often discernible when imaging the entire crystal. It is interesting that a rhombohedral morphology, which is a characteristic of calcite crystals grown in bulk solution, is still produced even when crystals are precipitated within the polymer network. The diffusion-limiting nature of gyroid network may play a role in the evolution of the long-ranged morphology, as will be addressed in a future publication.

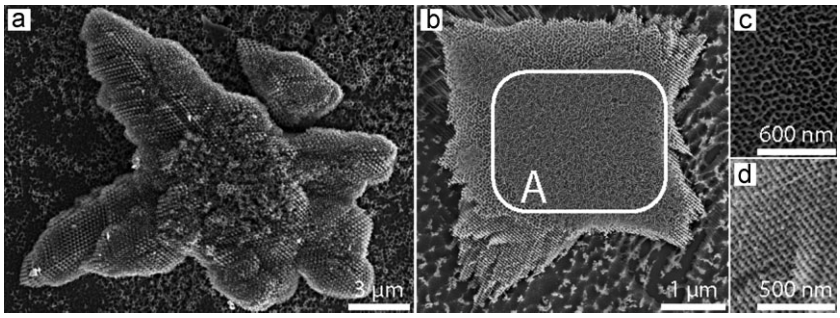

Figure 3. Gyroid-structured calcite single crystals that have nucleated and grown entirely within the confines of the polymer template as schematically illustrated in Figure 1f, Route B. a) A calcite crystal supported on the original substrate after removal of the polymer scaffold and b) the underside of an equivalent crystal, showing the crystal face originally in contact with the substrate. A disordered structure (marked A) is viewed, reflecting the disordered morphology of the copolymer film adjacent to the substrate surface. c–d) High-magnification images of (b).

A number of factors strongly suggested that the particles produced were single-crystalline calcite. In addition to the crystal overgrowth shown in Figure 2a and discussed earlier, examination of the crystals shown in Figure 3 between crossed polarizers in an optical microscope revealed a simultaneous intensity change of the entire crystal upon rotation of the analyzer, which is strongly indicative of single-crystal character. Confirmation that the templated particles were single crystals of calcite was obtained using electron diffraction. The sample shown in Figure 3a was

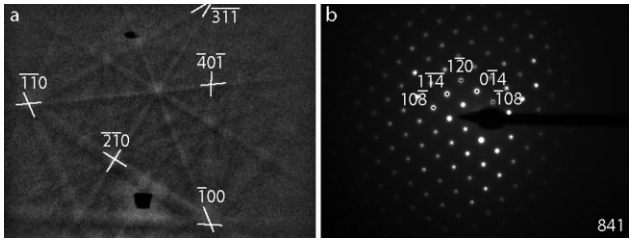

Figure 4. Analysis of the single-crystal particle shown in Figure 3a. a) Indexed Kikuchi bands corresponding to a calcite single crystal. The Kikuchi pattern is invariant with respect to the electron-beam focus on the crystal. b) Indexed electron-diffraction pattern of the crystal. The zone axis corresponds to the ⟨841⟩ direction, as indicated in the lower right corner.

characterized using electron backscatter diffraction (EBSD) and electron diffraction in a transmission electron microscope (TEM). The Kikuchi bands produced under EBSD are shown in Figure 4a. These arise from the backscattered diffraction of electrons of a focused electron beam incident on a single crystal. The intersections of the Kikuchi bands correspond to the intersection of zone axes in the crystal with the plane of observation, and can therefore be indexed with direct-lattice indices, which are indicative of the crystal symmetry. The indices marked in the Kikuchi pattern shown in Figure 4a are consistent with single-crystalline calcite, and the bands remained unchanged as the 5 nm beam was moved across the crystal. In comparison, polycrystalline Kikuchi patterns were seen when neighboring polycrystalline $CaCO_3$ aggregates were probed. Selected-area electron diffraction (1 μm diameter aperture) in a TEM was also used to examine the crystal shown in Figure 3a, and the patterns obtained confirmed that the entire particle was a single crystal of calcite, shown in Figure 4b. Thus, despite their morphological complexity, each templated particle is a single crystal of calcite.

The data therefore clearly show that nanostructured calcite single crystals can be readily prepared by a templating route when ACC is present as a precursor phase. When ion-by-ion growth is the principal mechanism (at concentrations <50 mM), limited penetration of the crystal into the polymer scaffold was observed as diffusion of the reactant ions is significantly retarded within the nanoscale pores of the template. In contrast, when ACC was present, significant crystal penetration into the polymer was observed, and indeed, the penetration depth increased with an increasing ion and therefore ACC concentration. These results are consistent with those of Li and Qi,[24] who showed that ACC is a required precursor to the formation of templated single crystals of calcite within colloidal crystals of polymer spheres. A key point is that ACC particles can effectively penetrate the relatively small gyroid structure completely and conformally. In this way, a large, continuous volume of the mold is filled with the precursor material prior to the onset of nucleation; the reactant material is in place and crystallization is not limited by diffusion of ions into the polymer scaffold. To generate single crystals, nucleation must then occur at a single point,[38] and crystallization presumably occurs isotropically via dehydration and mass transport.[15]

In summary, we have reported a straightforward process for fabricating nanostructured calcite single crystals with the double-gyroid morphology. Single-crystal formation occurred via an amorphous precursor phase that infiltrates the nanoporous polymer network, faithfully replicating its 30 nm features. Our strategy uses copolymer self-assembly, a proven and reliable method for the manufacture of tunable nanoporous bicontinuous films, to fashion polymer templates to direct crystal growth. While previous work has employed a native biomineral—sea-urchin skeletal plates—to produce templated single crystals with gyroid structures, as a synthetic method this technique was limited by the initial requirement for the biomineral and by the associated lack of control over its size and structure. Use of block-copolymer templates therefore represents a significant step forward to developing a general strategy for synthesizing crystals with complex forms, where the overall size of the crystal, and the geometry and periodicity of their internal structures are all controllable features.

Experimental Details

The polymers used were PS-*b*-PI (Mn = 45 kg mol^{-1} -*b*- Mn = 39 kg mol^{-1}, Polymer Source), and PS homopolymer (Mn = 8.7 kg mol^{-1}, Fluka).

Porous films were prepared by codissolving PS-*b*-PI and PS (overall PS volume fraction: 64%) in a toluene solution (10 wt% polymer). This solution (40 μL) was drop-cast onto a glass slide (2 cm^2) and covered with an ethylene tetrauoroethylene (ETFE) sheet (115 μm thick, Katco) to facilitate the formation of a crack-free homogeneously thick film. The sample was placed in a closed volume (4 cm^2) with a drop of toluene for seven days at 4 °C. In this setup, the solvent evaporated slowly during the course of a week, allowing the equilibration of the self-assembled nanostructure in the film. The films were then dried further in a vacuum oven at 40 °C for 12 h and irradiated with UV light (254 nm) for a further 12 h to crosslink the PS and degrade the PI, before the UV-transmitting EFTE sheets were removed. A short CF_4 plasma etch was used to remove a nonporous PS surface layer, followed by PI dissolution by immersion in ethanol for 12 h to expose the porous double-gyroid network.

$CaCO_3$ crystallization was initiated by submerging porous PS films, supported on glass, into a $CaCl_2$ aqueous/methanol solution (20 mL, 10 mM–1 M). The solution was 20 vol% methanol, to facilitate the infiltration of the solution into the porous polymer network. The crystallization vessel was placed in a closed desiccator containing a parafilm-sealed, needle-punctured vial of $(NH_4)_2CO_3$ powder to facilitate slow diffusion of CO_2 into the $CaCl_2$ solution. In some cases, polyacrylic acid (MW = 2 kg mol^{-1}, 10 μg mL^{-1}) was added to the growth solution to prolong the lifetime of the ACC. This promoted rounded features and secondary nucleation on the bulk calcite[16] although these remained single crystalline (as seen in electron diffraction), see Figure 2a. Crystal growth was quenched by removal of the substrate from the solution and washing in a 1:1 water/methanol solution for 1 min. The PS template was removed by heating at 385 °C under oxygen for 2 h. The heating step had no effect on the crystal morphology or crystallinity of the calcite: control experiments in which the PS was removed by oxygen-plasma etching yielded similar results.

For SEM analysis, the crystals were usually removed by adhesion on carbon tape. The crystal shown in Figure 3a was investigated on its substrate. The samples were sputter-coated with a 4 nm thick layer of amorphous carbon. SEM imaging was performed on a LEO 1530 operating at 5 kV. For TEM analysis, individual free-standing crystals were placed on a TEM grid using a micromanipulator.

EBSD analysis was performed using a Camscan MX2600 FESEM with a Nordlys EBSD detector using HKL Channel 5 software. The source electron beam had a width of 5 nm, the acceleration voltage was 25 kV, and the beam current was 1 nA. Samples were sputter-coated with a 1 nm thick amorphous carbon layer to avoid charging. TEM imaging and TEM electron diffraction were carried out using a FEI Philips Tecnai 20 TEM system operating at 200 kV.

Raman spectrometry was carried out using a SE1000 (Mesophotonics, now D3 Technologies) operating at 785 nm, 5 mW.

Acknowledgements

The authors would like to thank J. J. Rickard and D. Nicol for their assistance with TEM and EBSD, B. Soares for TEM sample preparation help. The ETFE sheets were donated by Katco. We gratefully acknowledge the EPSRC for funding. This article is part of the Special Issue celebrating the 800th Anniversary of the University of Cambridge.

Received: February 20, 2009
Revised: June 19, 2009
Published online: August 28, 2009

[1] F. C. Meldrum, H. Cölfen, *Chem. Rev.* **2008**, *108*, 4332.
[2] G. Donnay, D. Pawson, *Science* **1969**, *166*, 1147.
[3] J. Aizenberg, A. Black, G. Whitesides, *J. Am. Chem. Soc.* **1999**, *121*, 4500.

[4] A. Travaille, L. Kaptijn, P. Verwer, B. Hulsken, J. Elemans, R. Nolte, H. van Kempen, *J. Am. Chem. Soc.* **2003**, *125*, 11571.
[5] S. Mann, B. R. Heywood, S. Rajam, J. D. Birchall, *Nature* **1988**, *334*, 692.
[6] E. M. Pouget, P. H. H. Bomans, J. A. C. M. Goos, P. M. Frederik, G. de With, N. A. J. M. Sommerdijk, *Science* **2009**, *323*, 1555.
[7] E. Loste, E. Diaz-Marti, A. Zarbakhsh, F. Meldrum, *Langmuir* **2003**, *19*, 2830.
[8] S. Kwak, E. DiMasi, Y.-J. Han, J. Aizenberg, I. Kuzmenko, *Cryst. Growth Des.* **2005**, *5*, 2139.
[9] S. Raz, P. Hamilton, F. Wilt, S. Weiner, L. Addadi, *Adv. Funct. Mater.* **2003**, *13*, 480.
[10] P. Ajikumar, S. Vivekanandan, R. Lakshminarayanan, S. Jois, R. Kini, S. Valiyaveettil, *Angew. Chem. Int. Ed.* **2005**, *44*, 5476.
[11] G. Falini, S. Albeck, S. Weiner, L. Addadi, *Science* **1996**, *271*, 67.
[12] G. Fu, S. Qiu, C. Orme, D. Morse, J. D. Yoreo, *Adv. Mater.* **2005**, *17*, 2678.
[13] Y. Politi, T. Arad, E. Klein, S. Weiner, L. Addadi, *Science* **2004**, *306*, 1161.
[14] Y. Levi-Kalisman, S. Raz, S. Weiner, L. Addadi, I. Sagi, *Adv. Funct. Mater.* **2002**, *12*, 43.
[15] J. Aizenberg, D. Muller, J. Grazul, D. Hamann, *Science* **2003**, *299*, 1205.
[16] X.-R. Xu, A.-H. Cai, R. Liu, H.-H. Pan, R.-K. Tang, K. Cho, *J. Cryst. Growth* **2008**, *310*, 3779.
[17] J. D. Rodriguez-Blanco, S. Shaw, L. G. Benning, *Mineral. Mag.* **2008**, *72*, 283.
[18] B. Wucher, W. Yue, A. N. Kulak, F. C. Meldrum, *Chem. Mater.* **2007**, *19*, 1111.
[19] W. Yue, A. N. Kulak, F. C. Meldrum, *J. Mater. Chem.* **2006**, *16*, 408.
[20] R. J. Park, F. C. Meldrum, *J. Mater. Chem.* **2004**, *14*, 2291.
[21] N. Hetherington, A. N. Kulak, K. Sheard, F. C. Meldrum, *Langmuir* **2006**, *22*, 1955.
[22] S. Ludwigs, U. Steiner, A. N. Kulak, R. Lam, F. C. Meldrum, *Adv. Mater.* **2007**, *18*, 2270.
[23] F. C. Meldrum, S. Ludwigs, *Macromol. Biosci.* **2007**, *7*, 152.
[24] C. Li, L. Qi, *Angew. Chem. Int. Ed.* **2008**, *47*, 2388.
[25] I. W. Hamley, in *The Physics of Block Copolymers*, Oxford Science Publications, UK **1998**.
[26] D. Hajduk, P. Harper, S. Gruner, C. Honeker, G. Kim, E. Thomas, L. Fetters, *Macromolecules* **1994**, *27*, 4063.
[27] M. Schultz, F. Bates, K. Almdal, K. Mortensen, *Phys. Rev. Lett.* **1994**, *73*, 86.
[28] A. Khandpur, S. Forster, F. Bates, I. Hamley, A. Ryan, W. Bras, K. Almdal, K. Mortensen, *Macromolecules* **1995**, *28*, 8796.
[29] M. Lai, A. N. Kulak, D. Law, Z. Zhang, F. C. Meldrum, D. J. Riley, *Chem. Commun.* **2007**, *34*, 3547.
[30] S. Torquato, A. Donev, *Proc. Roy. Soc. Lond. A Mater.* **2004**, *460*, 1849.
[31] S. Torquato, S. Hyun, A. Donev, *J. Appl. Phys.* **2003**, *94*, 5748.
[32] H. Tanaka, H. Hasegawa, T. Hashimoto, *Macromolecules* **1991**, *24*, 240.
[33] H. Mao, M. Hillmyer, *Soft Matter* **2006**, *2*, 57.
[34] T. Hashimoto, Y. Nishikawa, K. Tsutsumi, *Macromolecules* **2007**, *40*, 1066.
[35] L. Addadi, J. Moradian, E. Shay, N. Maroudas, S. Weiner, *Proc. Natl. Acad. Sci. USA* **1987**, *84*, 2732.
[36] H. Lee, T. Ha, K. Kim, *Mater. Chem. Phys.* **2005**, *93*, 376.
[37] R. Seshadri, F. Meldrum, *Adv. Mater.* **2000**, *12*, 1149.
[38] E. Loste, R. J. Park, J. Warren, F. C. Meldrum, *Adv. Funct. Mater.* **2004**, *14*, 1211.